Electronic Supplementary Material (ESI) for Journal of Materials Chemistry B.

Supporting Information

In-situ engineering of Au-Ag alloy embedded PEDOT nanohybrids at a solvent/non-solvent interface for the electrochemical enzyme-free detection of histamine

Nesleena Puthiyottil[a], Sameena Kanakkayil[a], Neeraja P Pillai[a], Anju Rajan[b], Sijina Kinattingara Parambath[c], Rajanikant Golgodu Krishnamurthy[c], Raghu Chatanathodi[b], Mini Mol Menamparambath [a]*

[a]Department of Chemistry, National Institute of Technology Calicut, Calicut-673601, Kerala, India.
[b]Department of Physics, National Institute of Technology Calicut, Calicut-673601, Kerala, India.
[c]School of Biotechnology, National Institute of Technology Calicut, Calicut-673601, Kerala, India.

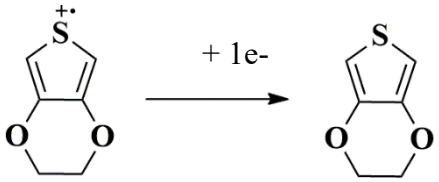

EDOT radical cation **EDOT** E^o_P **= - 3.95 V**[1]

Sl. No.	Metal ion conversion	Standard Reduction Potential of Metal *vs.* NHE E^o_M (V)	No of electrons involved in the reaction, (n)	E^o_{cell} (V) = $E^o_M - E^o_P$	Standard Gibbs free energy, $\Delta G°$ (kcalmol^{-1})
1.	$Ag^+ + 1e^- \rightarrow Ag^0$	0.80[2]	1	4.75	-109.5
2.	$Au^{3+} + 3e^- \rightarrow Au^0$	0.99[3]	3	4.94	-341.6

Supporting Table S1. Table showing the half-cell reaction of metal ions at the cathode, standard reduction potentials of monomer (E°_P) and metal ions (E°_M), number of electrons (n) involved in the redox reaction and the electrochemical cell potential (E°_{cell}). The thermodynamic free energy, $\Delta G° = -nFE^{\circ}_{cell}$ was calculated to predict the thermodynamic feasibility of polymerization reactions.

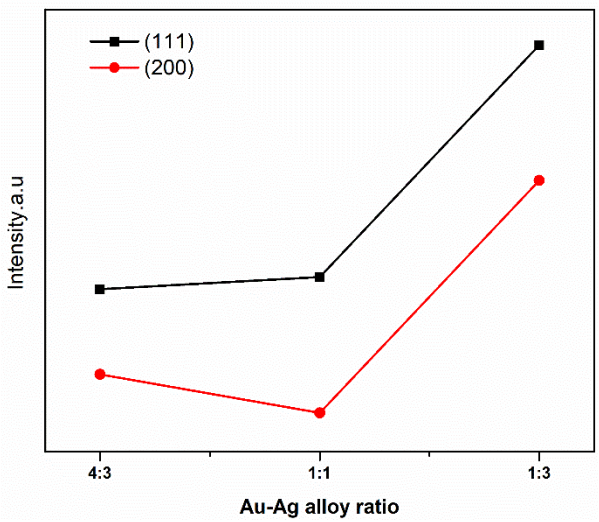

Supporting Fig. S1. Comparison of the variation in diffraction plane intensity of PEDOT/Au-Ag alloy with change in Au^{3+}/Ag^{+} ratios.

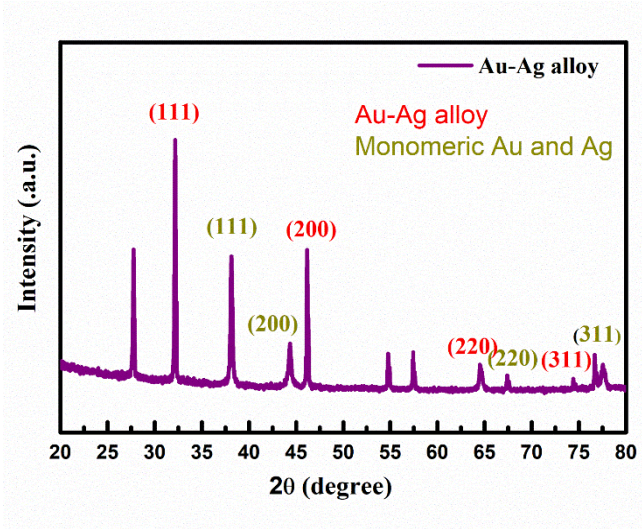

Supporting Fig. S2. XRD spectra of Au-Ag alloy formed by the simple mixing of $HAuCl_4$ and $AgNO_3$ solutions in 1: 3 ratio.

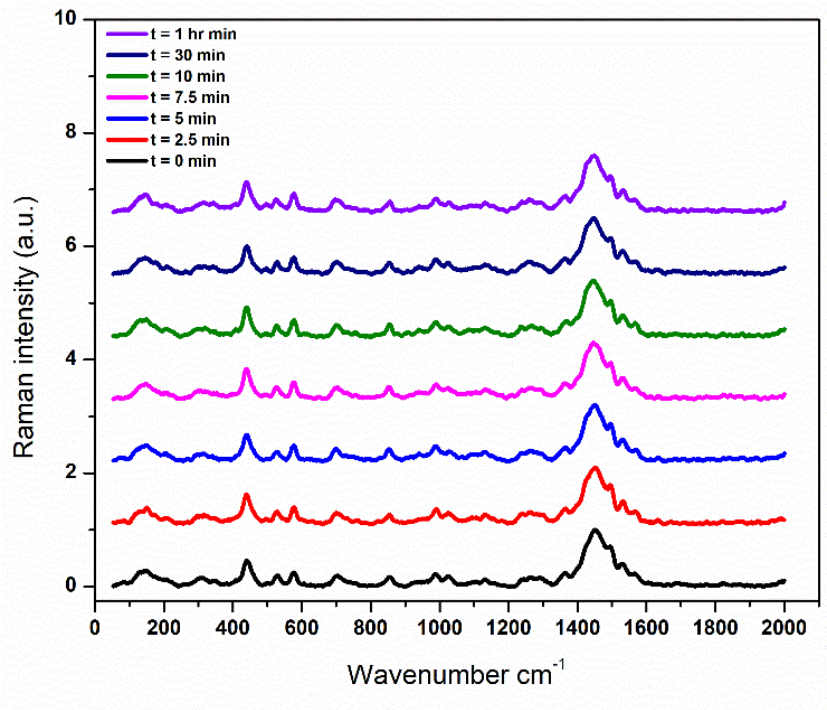

Supporting Figure S3. Raman spectra of PEDOT/Au-Ag alloy synthesized at various time intervals from t = 0 to t = 1 hr

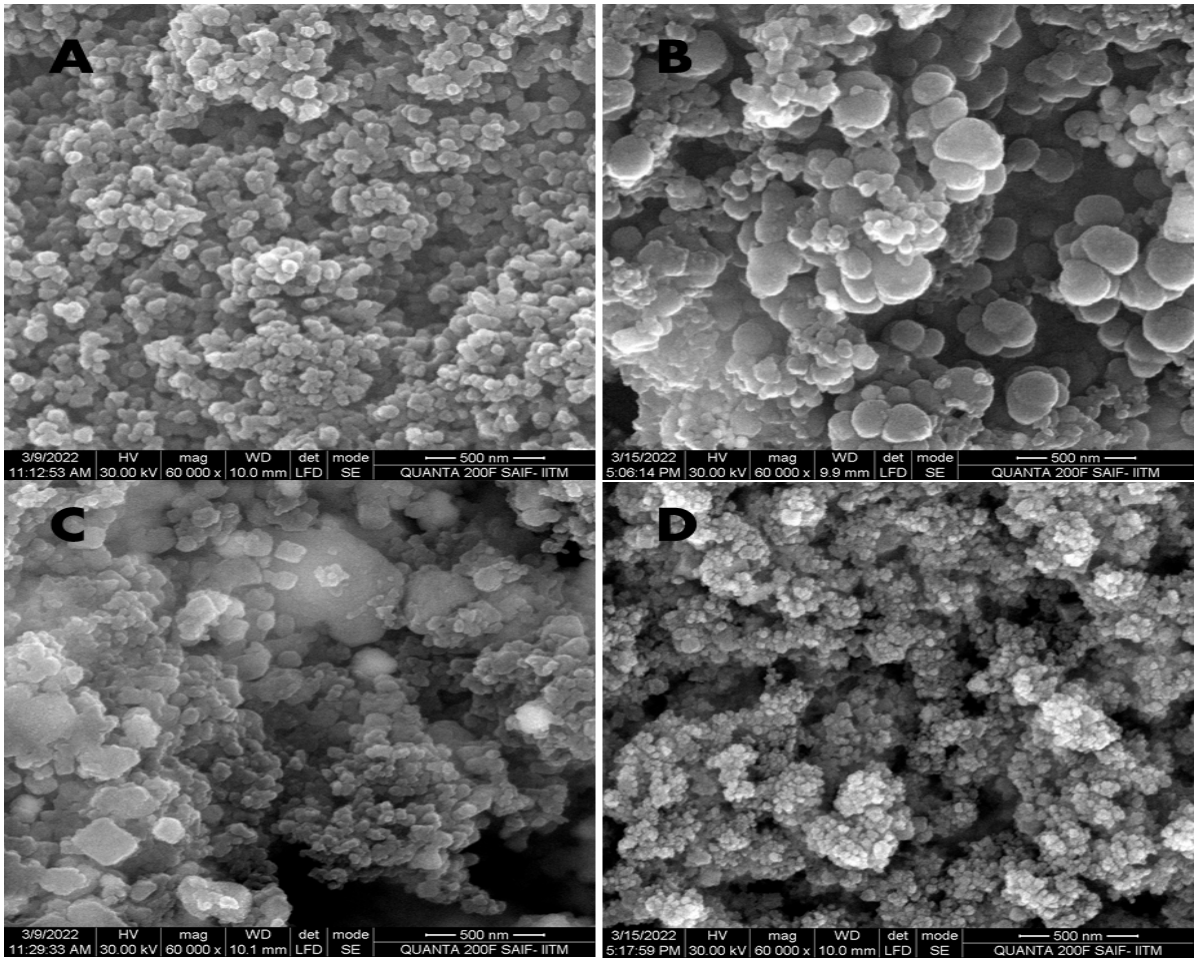

Supporting Fig. S4. SEM Images of PEDOT:Au-Ag alloy samples made with different Au/Ag mole ratios. (A) SEM image of PEDOT:Au without Ag, (B) SEM image of PEDOT alloy with Au/Ag mole ratio of 1:1, (C) Au/Ag mole ratio 4:3 and (D) Au/Ag mole ratio 1:3

It can be noted that the optimized product PEDOT/Au- Ag (1:3) has smaller uniformly sized particles compared to the FE-SEM images of other compositions. It is reported that the Au^{3+}/Ag^{+} molar ratio affects the average size of Au–Ag alloy NPs formed.[4]

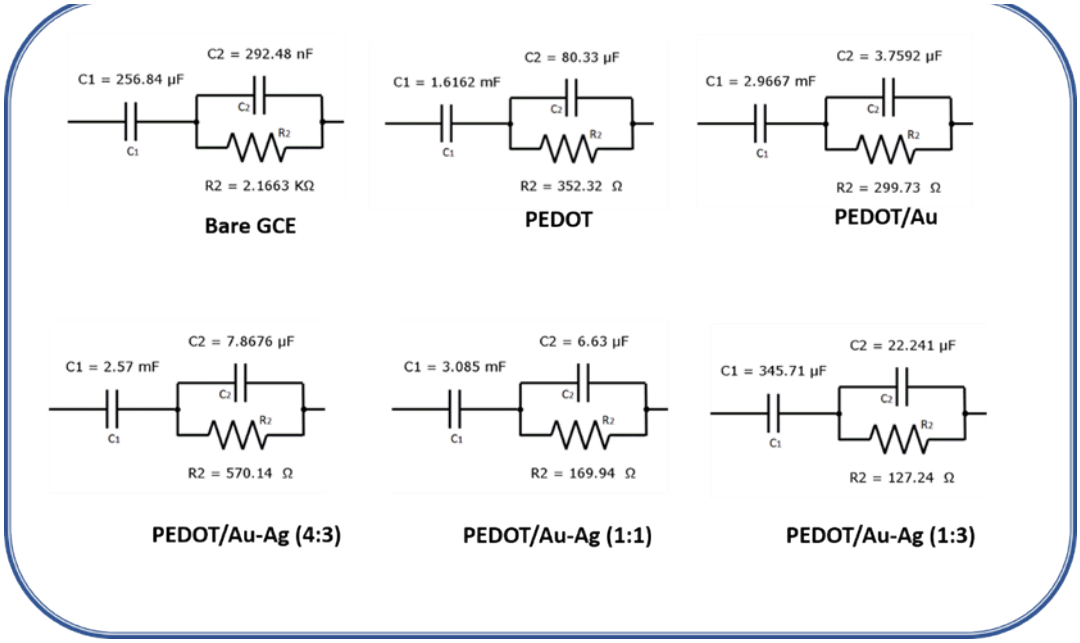

Supporting Fig. S5. The equivalent circuit diagrams corresponding to the Nyquist plots shown in Fig. 2d.

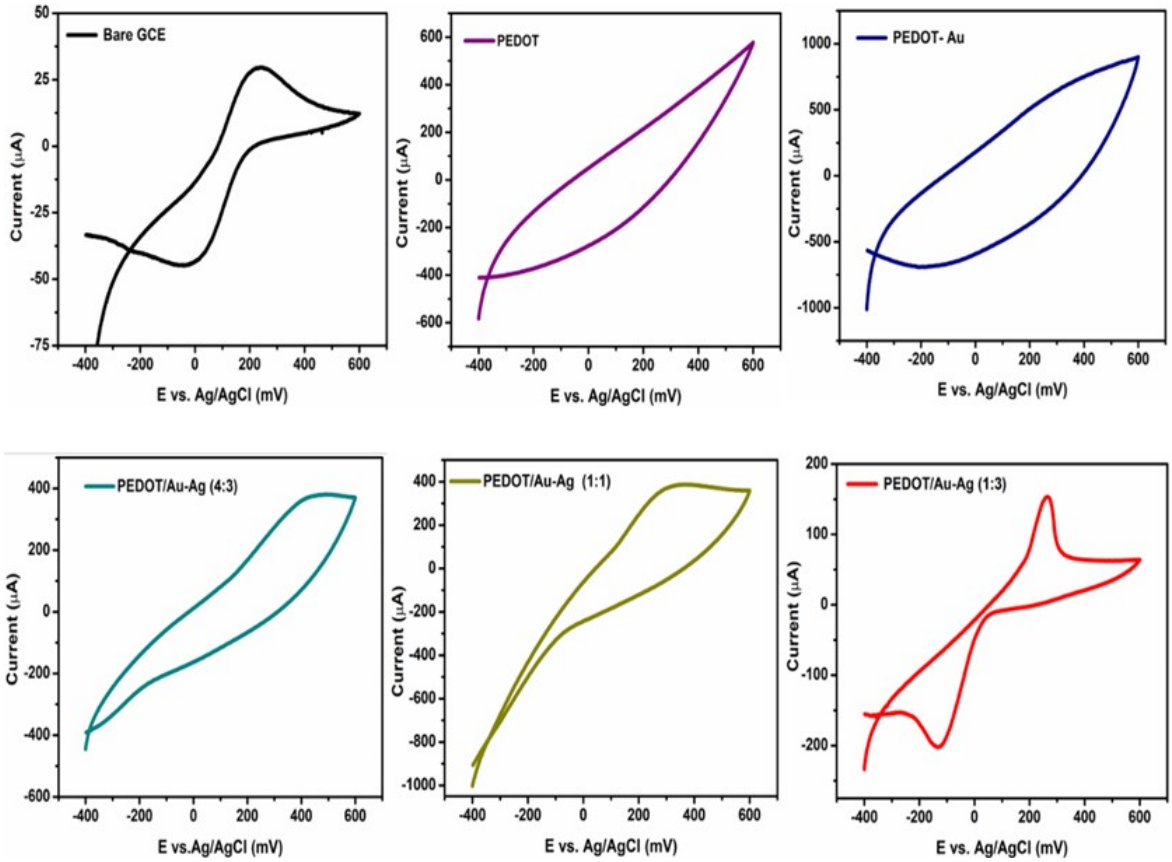

Supporting Fig. S6. Comparison of the electrochemical activity of Bare GCE, PEDOT, PEDOT- Au, and PEDOT/Au-Ag alloys with Au^{3+}/Ag^{+} mole ratio (4:3), (1:1) and (1:3) in 5mM $K_4[Fe(CN)_6]$ in 0.1MKCl.

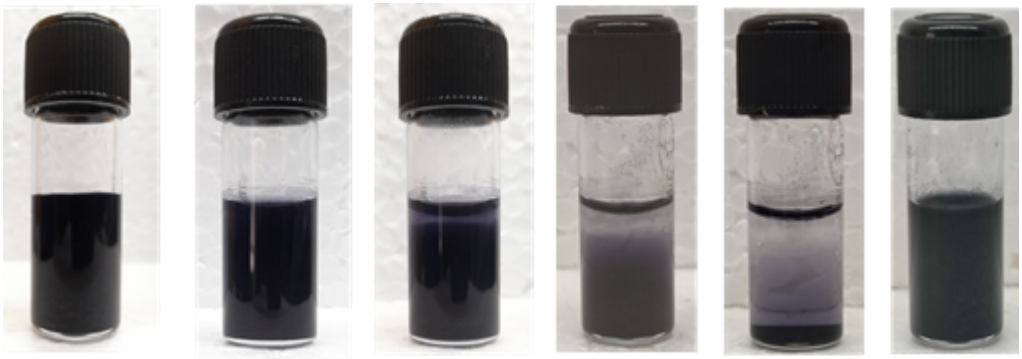

Day 1 Day 5 Day 10 Day 15 Day 20 After shaking

Supporting Fig. S7. Dispersion stability of PEDOT/Au-Ag (1:3) in water

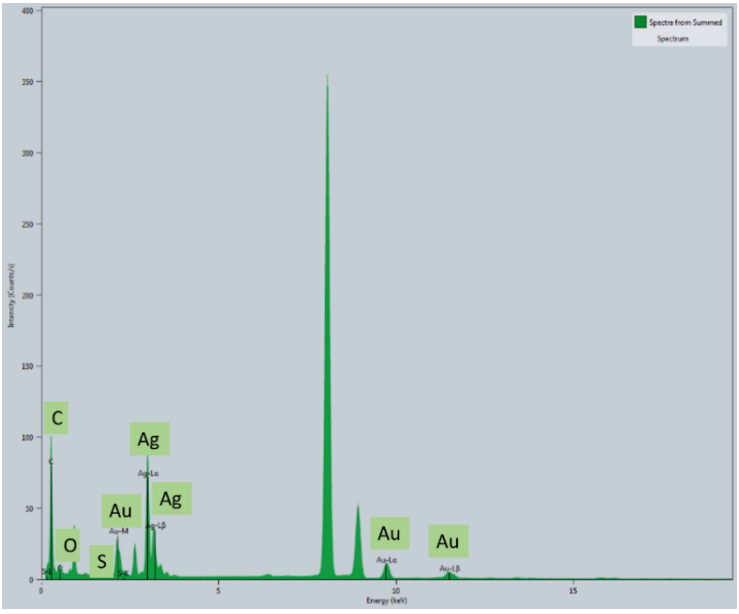

Supporting Fig. S8. HRTEM-EDS spectrum of PEDOT/Au-Ag alloy (1:3)

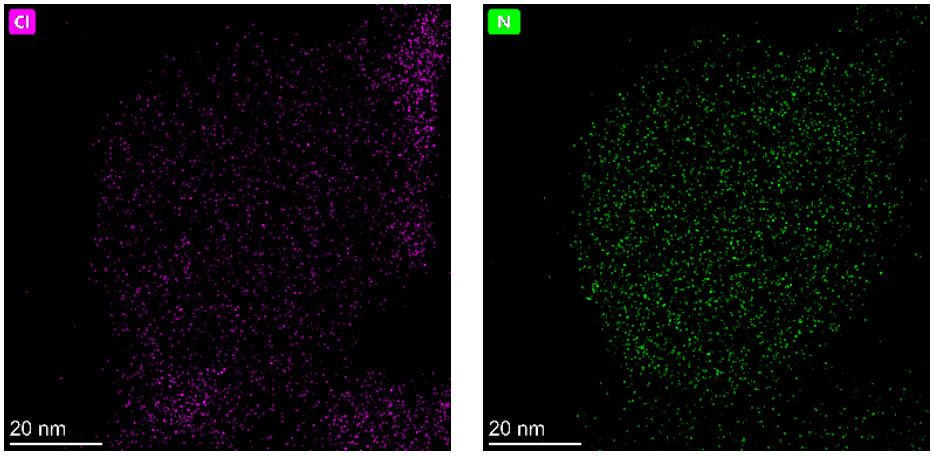

Supporting Fig. S9. Elemental mapping images of Chlorine and Nitrogen present in PEDOT/Au-Ag (1:3)

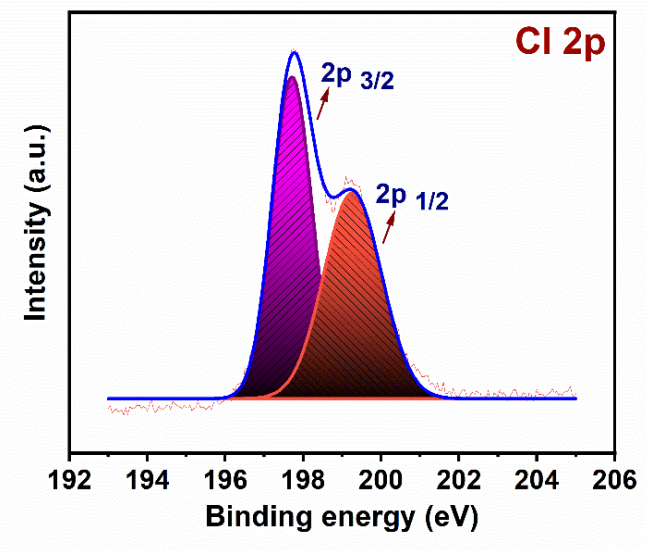

Supporting Fig. S10. XPS spectra of Chlorine

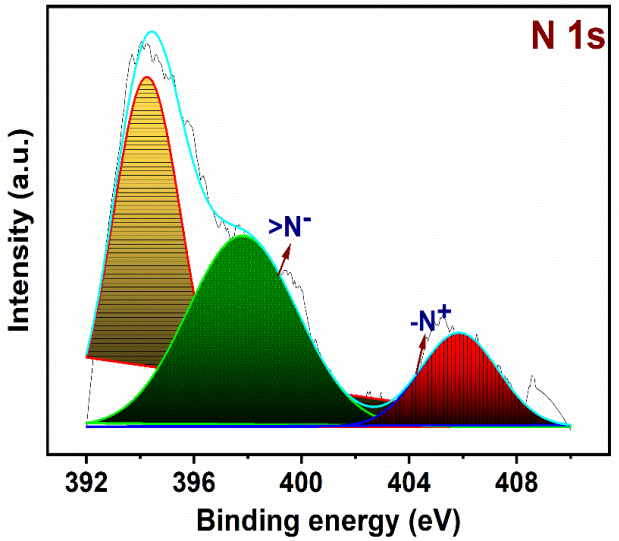

Supporting Fig. S11. XPS spectra of Nitrogen

Sl. No.	Type of material	Detection technique	Linear range	Oxidation peak potential (V)	LOD	Ref.
1	Au-NPs	Fluorescence	0.01–1.0 μM	Not applicable	2.04 nM	S5
2	Ag-Ag_2O/ MWCNTs/GCE	DPV	5-200 mM	0.97	0.018 μM	S6
3	Au NPs	Colorimetry (LSPR)	0.4-2.63 mM	Not applicable	38 nM	S7
4	rGO-ppy/GCE	DPV	10-800 μM	0.67	3.01μM	S8
5	TGA-CdTe QDs	Fluorescence	9.6-570 μM	Not applicable	9.6 μM	S9
6	Cu@Pd core shell NPs	Amperometry	0.1-10 μM	0.55	3.2 nM	S10
7	Nafion-MWCNTs/GCE	DPV	20-200 μM	1.12	0.39 μM	S11
8	MIP/L-cysteine/AuNPs /GCE	DPV	1-107 μM	1.2	0.6 μM	S12
9	MIP-apt/AuNPs /CNT/GCE	EIS	0.35-35 nM	0.3	0.11 nM	S13
10	MWCNTs/CPE	DPV	0.1-100 μM	1.12	1. 26 μM	S14
11	BDD electrode	CV	0.5–100 μM	1.4	0.5 μM	S15
12	Lingnin/GCE	CV	5-200 μM	1.35	0.38 μM	S16
13	SWCNT/CPE	DPV	4.5- 720 μM	1.25	1.26 μM	S17
14	FrGO/GCE	Amperometry	0.2-80 μM	0.74	0.007 μM	S18
15.	**PEDOT/Au-Ag (1:3) alloy Present work**	**CV**	**100 nM - 1 μM**	**0.13**	**1.25 nM**	

Supporting Table S2. Performance comparison of PEDOT/Au-Ag (1:3) sensor for HA detection with other previously reported sensors.

Sl. No.	Materials	Synthesis method	Analyte	Detection technique	LOD	Ref.
1.	PEDOT/NiNPs/GO	Electro-polymerization	Glucose	Amperometry	0.8 μM	S19
2.	PEDOT/PEDOT-SH/Au	Electro-polymerization	Nitrite	Amperometry	0.051 μM	S20
3.	PEDOT/PdNPs	Chemical Oxidation	Peroxide	Amperometry	2.84 μM	S21
4.	PtNPt/MWCNT-PEDOT:PSS	Electrochemical method	DA	CV	50 nM	S22
5.	PEDOT:PSS-RGO/AuNPs	Chemical oxidation	Peroxide	Amperometry	0.08 μM	S23
6.	PEDOT-PPY/Ag	Chemical oxidation	DNA	EIS	5.4 fM	S24
7.	PEDOT/GO/CuNPs	Electrochemical method	Glucose	Amperometry	47 nM	S25
8.	PEDOT/CNTs/ Cu-Co	Electrochemical method	Nitrite	Amperometry	60 nM	S26
9.	PEDOT/Ag NPs	Electrochemical method	Caffeic acid	CV	1.9 μM	S27
10.	PEDOT /AuNPs /CNT	Chemical oxidation	AA and UA	CV, DPV	0.283 μM	S28
11.	**PEDOT/Au-Ag alloy Present work**	**Liquid-liquid interface-assisted polymerization**	**HA**	**CV**	**1.5 nM**	

Supporting Table S3. The synthesis method and performance comparison of PEDOT-based composites for the non-enzymatic detection of various analytes.

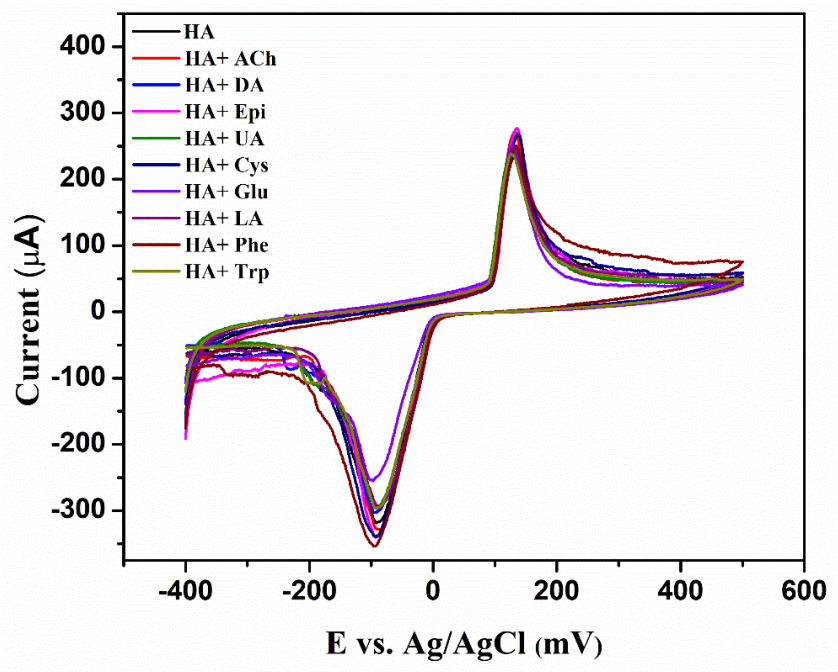

Supporting Fig. S12. Cyclic Voltammograms of PEDOT/Au-Ag (1:3) in 100μM HA in the presence of various interfering groups at a scan rate of 50mV/s

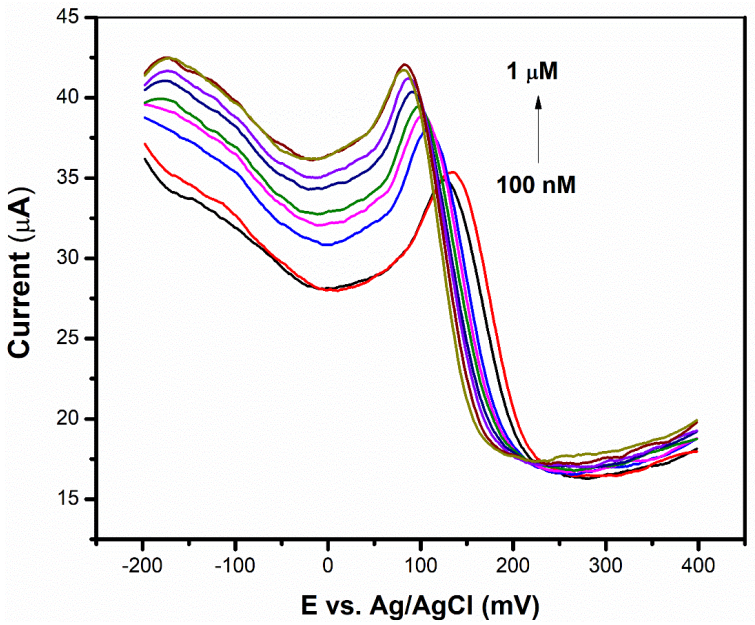

Supporting Fig. S13. DPV plots of PEDOT/Au-Ag (1:3) modified GCE towards varying concentrations of HA

Sl. No.	Added Concentration (nM)	Output current in std soln (µA)	Output current in fish extract solution (µA)	Recovery Concentration (nM)	% Recovery	RSD (%)
1	0	_	35	106	_	_
2	500	39.5	36	378	75.6	1.89
3	600	40.36	38.7	451	75.1	1.65
4	700	41.2	41.47	723	103.28	2.65
5	800	41.7	43.37	899	112.37	1.74
6	900	42	44.82	992	110.2	2.14
7	1000	43.5	45.97	1110	111.0	2.81

Supporting Table S4. Recovery results of HA in Canned Tuna Fish.

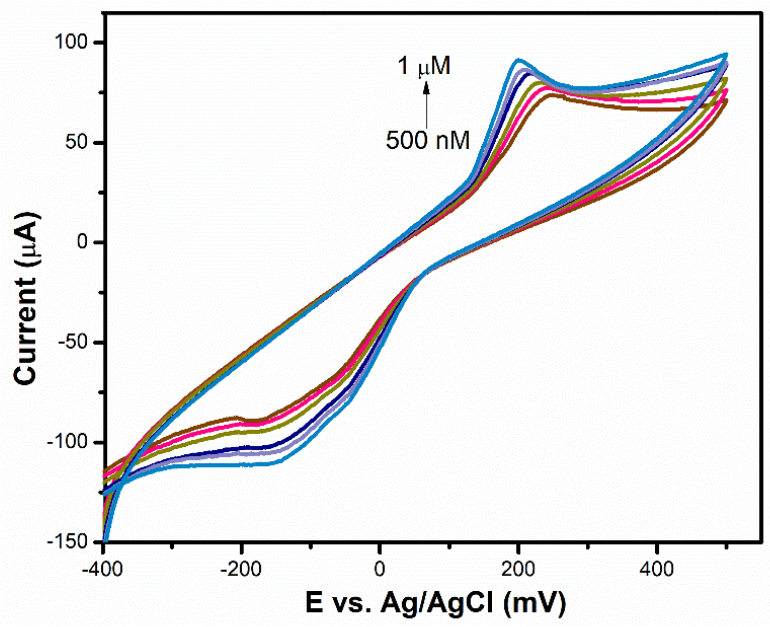

Supporting Fig. S14. CV plots of PEDOT/Au-Ag (1:3) modified GCE at different concentrations of HA in artificial sweat sample

Sl No.	Added Concentration (nM)	Output current in std soln (µA)	Output current in serum sweat solution (µA)	Recovery Concentration (nM)	% Recovery	RSD (%)
	Added Concentration (µM)	Output current in std soln (µA)	Output current in artificial sweat solution (µA)	Recovery Concentration (µM)	Recovery	RSD (%)
1	50	175	174	55	110	2.9
1	500	111	115.3	401	80.2	2.89
2	60	187	180.7	72	120	2.7
2	600	113	117.76	496	82.6	2.5
3	70	191	187	77	110	2.9
3	700	118	122.08	627	89.5	3.1
4	80	192	192	79	98.7	1.95
4	800	121	125.77	727	90.8	3.5
5	90	195	197.2	84	93.33	3.85
5	900	123	129.47	794	88.5	2.47
6	100	197	200.7	86	86	2.91
6	1000	129	131.52	1004	100.4	1.81

Supporting Table S5. Recovery results of HA in artificial sweat sample.

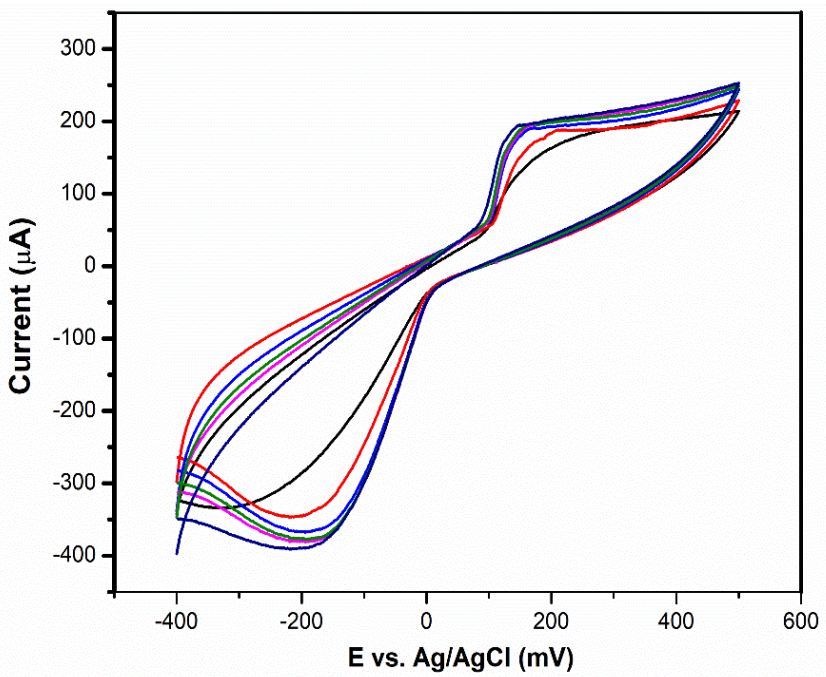

Supporting Fig. S15. CV plots of PEDOT/Au-Ag (1:3) modified GCE at different concentrations of HA in human serum.

Supporting Table S6. Recovery results of HA in human serum sample.

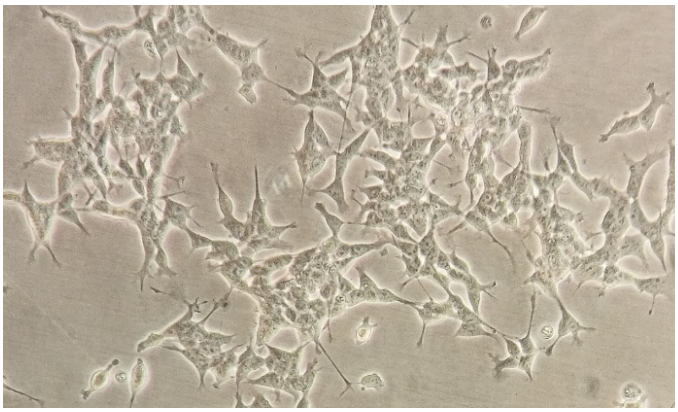

Supporting Fig. S16. Microscopic image of SH-SY5Y neural cells cultured in DMEM medium after two hrs of the addition of L-Histidine precursor.

References

S1 S. Lee and H. Lee, *J. Electrochem. Sci. Technol.*, 2012, **3**, 85–89.

S2 P. Arul, S. T. Huang, V. Mani and C. H. Huang, *ACS Appl. Nano Mater.*, 2022, **5**, 6340–6351.

S3 N. S. K. Gowthaman, B. Sinduja and S. A. John, *RSC Adv.*, 2016, **6**, 63433–63444.

S4 L. Sun, Y. Yin, P. Lv, W. Su and L. Zhang, *RSC Adv.*, 2018, **8**, 3964–3973.

S5 J. Bi, C. Tian, G. L. Zhang, H. Hao and H. M. Hou, *Foods*.

Supporting Fig. S17. Image showing the electrochemical detection set up for the detection of HA released by human neural cells using DPV technique.

S6 N. Butwong, J. Khajonklin, A. Thongbor and J. H. T. Luong, *Microchim. Acta*, ,

S7 C. Huang, S. Wang, W. Zhao, C. Zong, A. Liang, Q. Zhang and X. Liu, *Microchim. Acta*, 2017, **184**, 2249–2254.

S8 B. Hu, N. Zhang, H. Li and C. Sun, *Int. J. Electrochem. Sci.*, 2021, **16**, 1–13.

S9 S. Khan, L. S. A. Carneiro, M. S. Vianna, E. C. Romani and R. Q. Aucelio, *J. Lumin.*, 2017, **182**, 71–78.

S10 Z. Wu, E. Xu, A. Jiao, Z. Jin and J. Irudayaraj, *RSC Adv.*, 2017, **7**, 44933–44944.

S11 R. K. R. Gajjala and S. K. Palathedath, *Biosens. Bioelectron.*, 2018, **102**, 242–246.

S12 S. Li, T. Zhong, Q. Long, C. Huang, L. Chen, D. Lu, X. Li, Z. Zhang, G. Shen and X. Hou, *Microchem. J.*, 2021, **171**, 106844.

S13 A. M. Mahmoud, S. A. Alkahtani, B. A. Alyami and M. M. El-Wekil, *Anal. Chim. Acta*, 2020, **1133**, 58–65.

S14 A. Geto, M. Tessema and S. Admassie, *Synth. Met.*, 2014, **191**, 135–140.

S15 B. V Sarada, T. N. Rao, D. A. Tryk and A. Fujishima, *Anal. Chem.*, 2000, **72**, 1632–1638.

S16 H. Degefu, M. Amare, M. Tessema and S. Admassie, *Electrochim. Acta*, 2014, **121**, 307–314.

S17 Z. S. Stojanović, E. Mehmeti, K. Kalcher, V. Guzsvány and D. M. Stanković, *Food Anal. Methods*, 2016, **9**, 2701–2710.

S18 F. Shahzad, S. A. Zaidi and C. M. Koo, *ACS Appl. Mater. Interfaces*, 2017, **9**, 24179–24189.

S19 N. Hui, S. Wang, H. Xie, S. Xu, S. Niu and X. Luo, *Sensors Actuators B. Chem.*, 2015, **221**, 606–613.

S20 Y. Ge, R. Jamal, R. Zhang, W. Zhang, Z. Yu, Y. Yan and Y. Liu, 2020, 1–10.

S21 F. Jiang, R. Yue, Y. Du, J. Xu and P. Yang, *Biosens. Bioelectron.*, 2013, **44**, 127–131.

S22 Z. Lu, S. Xu, H. Wang, E. He, J. Liu, Y. Dai, J. Xie, Y. Song, Y. Wang, Y. Wang, L. Qu and X. Cai, *ACS Appl. Bio Mater.*, 2021, **4**, 4872–4884.

S23 S. Correa, *Appl. Surf. Sci.*

S24 S. Radhakrishnan, C. Sumathi, A. Umar, S. Jae, J. Wilson and V. Dharuman, *Biosens. Bioelectron.*, 2013, **47**, 133–140.

S25 N. Hui, W. Wang and X. Luo, 2015, 556–561.

S26 J. Wang, G. Xu, W. Wang, S. Xu and X. Luo, *Chem. - An Asian J.*, 2015, **10**, 1892–1897.

S27 J. J. García-Guzmán, D. López-Iglesias, L. Cubillana-Aguilera, D. Bellido-Milla, J. M. Palacios-Santander, M. Marin, S. D. Grigorescu, C. Lete and S. Lupu, *Electrochim. Acta*

S28 Chen, W. Chen, Y. Wang, X. Wang, Y. Ding, D. Zhao and J. Liu, *RSC Adv.*, 2022, **12**, 15038–15045.

-